Li *et al. Genome Medicine* (2026) 18:68
https://doi.org/10.1186/s13073-026-01641-x

Genome Medicine

RESEARCH Open Access

# Single cell multiomics revealed fibrotic trajectories of endometrial cells and interaction with the pro-fibrotic macrophages in intrauterine adhesion

Yu Li[1,2*†], Wei Wu[4†], Houyi Lv[1†], Libing Shi[3†], Zhuomin Wang[1], Chengcheng Zhu[1], Junwen Zhang[1], Xilin Shen[4], Yiyuan Qu[1], Wanwan Xu[1], Shunxian Ji[1], Ying Gu[1], Mohammad Ishraq Zafar[1], Yingying Hu[1], Xiao Chen[1], Xiaofeng Zhao[1], Songying Zhang[3*], Jian Xu[1,4*] and Bingbing Wu[1*]

## Abstract

**Background** Intrauterine adhesion (IUA) is prevalent in women of childbearing age and can affect pregnancy outcomes or even lead to infertility. Currently, there is no effective clinical cure.

**Methods** We profiled more than 100, 000 human endometrial cells from IUA and normal endometrial tissues using single cell RNA sequencing (scRNA-seq), single nucleus transposase-accessible chromatin sequencing (snATAC-seq) and spatial transcriptomics to gain an in-depth understanding of the cellular and molecular mechanisms underlying IUA pathogenesis and enable the development of therapeutic targets.

**Results** We investigated the diversity of fibrotic cell populations in human IUA. In addition to myofibroblasts, we identified a novel ACTA2 + KRT8+ myofibrotic-epithelial subpopulation and ACTA2 + CD31+ myofibrotic-endothelial subpopulation. The three fibrotic cell lineages were also detected in the rat IUA model. We also reconstructed the molecular differentiation trajectories and fibrotic molecular characteristics of the multiple fibrotic cell lineages. Extracellular matrix (ECM) related genes and fibrosis-related transcription factors (TFs) were highly expressed in the multiple fibrotic cell lineages in human and rat IUA. Finally, we revealed the pro-fibrotic immune microenvironment of IUA, in which the pro-fibrotic macrophage population was highly enriched in the IUA fibrotic niche and positively correlated with IUA clinical disease features. Macrophages can promote fibrotic gene expression in fibrotic cell

†Yu Li, Wei Wu, Houyi Lv and Libing Shi contributed are co-first author.

*Correspondence:
Yu Li
21418039@zju.edu.cn
Songying Zhang
zhangsongying@zju.edu.cn
Jian Xu
xuj@zju.edu.cn
Bingbing Wu
0012865@zju.edu.cn

Full list of author information is available at the end of the article

populations through SPP1 and GALECTIN9. The changes in the fibrotic immune microenvironment showed high consistency in the human and rat IUA endometrium.

**Conclusions** Our study resolved the contribution of multiple fibrotic cell lineages and their interactions with the pro-fibrotic macrophages to endometrial fibrosis in IUA and provided therapeutic targets for IUA treatment.

**Keywords** Intrauterine adhesion, Single cell RNA sequencing, SnATAC-seq, Spatial transcriptomics, Fibrotic cell populations, Macrophage

## Background

The endometrium is an important site for embryo implantation and development. Once risk factors such as miscarriages, infection, dilatation, and curettage damage the basal layer of the endometrium, it leads to defects in endometrial regeneration, and resulting in uterine fibrosis and scar adhesions. Approximately 19% of women with a history of miscarriage are diagnosed with intrauterine adhesions (IUA) or asherman's syndrome (AS) 12 months after surgery [1]. IUA not only causes secondary infertility in women, but also affects subsequent pregnancy outcomes. The spontaneous miscarriage rate in patients with IUA is 40%. The preterm birth rate is approximately 23%, the placental hyperplasia rate is approximately 13%, and the ectopic pregnancy rate is approximately 12% [2]. The reported pregnancy data for the general population showed that the overall risk of spontaneous abortion was 10.9% and the overall risk of ectopic pregnancy was 2.3% [3]. The pooled risk of miscarriage is 15.3% [4], which is much lower than the rate in patients with IUA.

At present, hysteroscopic surgery is the main clinical treatment strategy for the separation of IUA adhesions, and anti-adhesion gels such as hyaluronic acid are used to prevent the recurrence of adhesions [5]. However, the recurrence rate of severe IUA is still as high as 62.5%, and the successful pregnancy rate after surgery is only approximately 33.3% [6]. Recently, current tissue regeneration technologies based on stem cells and biomaterials have shown great promise in the regenerative therapy of IUA [7, 8]. However, the lack of in-depth research on the pathological cellular microenvironment and potential molecular mechanisms of IUA seriously hinders the research and development of new strategies for the prevention and treatment of this disease.

The occurrence and development of fibrosis are considered key driving factors of IUA [5, 9].The development of tissue fibrosis is caused by excessive deposition of the extracellular matrix by locally activated fibrotic cells [10]. Recently, fibrotic cell heterogeneity and functional diversity have been revealed in tissue fibrosis processes such as renal fibrosis [11], liver fibrosis [12] and skin scar formation [13]. Meanwhile, there has been an increasing research interest in the role of cell-cell interactions in the disease microenvironment during disease development [10]. Therefore, in this study, we reconstructed a single-cell multi-omics atlas of human IUA and investigated the diversity of fibrotic cell lineages and pro-fibrotic immune microenvironments in human and rat IUA. We generated a multi-lineage interactome in the fibrotic niche of IUA, in which SPP1 and LGALS9 secreted by macrophages promoted the fibrotic changes in endometrial cells. Our study resolved the conserved multiple fibrotic cell lineages and their pathogenic microenvironments in IUA, and provides therapeutic targets for developing effective strategies for IUA treatment.

## Methods

### Human IUA tissue collection

Human IUA endometrial samples were collected from biopsies of the adhesion tissue during the transcervical resection of adhesions after IUA scoring. According to the American Fertility Society (AFS) classification scoring criteria, patients with an AFS score of ≥ 3 who underwent hysteroscopy were diagnosed with IUA in our study and were included in the IUA group. Normal human endometrial samples for cell culture or snATAC-seq were collected from the biopsies of non-affected areas of the endometrium during myomectomy or endometrial polyp removal. The sampling protocol was uniform for all samples. All human samples were collected from the Fourth Affiliated Hospital, School of Medicine, Zhejiang University.

Cohort one: 12 IUA endometrial samples were collected for single cell analysis (9 for scRNA-seq, 3 for snATAC-seq), 6 normal human endometrial samples were collected as the normal control group for single cell analysis (3 for scRNA-seq, 3 for snATAC-seq). Details for the samples used for single cell analysis were summarized in Table S1 (Additional file 1). Approvals for utilizing the patient samples were obtained from the Ethics Committee of the Fourth Affiliated Hospital, School of Medicine, Zhejiang University (Approval Number: K2021042). Informed consents were obtained from all participants.

Cohort two: Additional samples for histological examination, including 11 normal endometrial samples and 39 IUA samples, clinical features for samples collected for histological analysis was summarized in Table S3 (Additional file 1). These samples were collected by fixing in paraffin wax from the pathology department of the

Fourth Affiliated Hospital. Approvals for the use of these samples were obtained from the Ethics Committee of the Fourth Affiliated Hospital, School of Medicine, Zhejiang University (Approval Number: K2021113). All the histological staining was performed on the tissue sections obtained through paraffin sectioning.

### Tissue dissociation and preparation

Fresh tissue specimens were washed with Hank's Balanced Salt Solution (HBSS) for three times and minced into 1–2 mm pieces. The tissue pieces were then digested with 2 mL GEXSCOPE® Tissue Dissociation Solution (Singleron) at 37℃ for 15 min in a 15 mL centrifuge tube with sustained agitation. After digestion, the samples were filtered using 40-micron sterile strainers and centrifuged at 1,000 rpm for 5 min. The supernatant was discarded, and the sediment was resuspended in 1 mL PBS (HyClone). To remove the red blood cells, 2 mL GEXSCOPE® red blood cell lysis buffer (Singleron) was added at 25 °C for 10 min. The solution was then centrifuged at 500 × g for 5 min and suspended in PBS. The samples were stained with trypan blue (Sigma) and microscopically evaluated.

### Single cell RNA sequencing, snATAC-seq and Visium V2 spatial transcriptomic analysis

#### *Single-cell RNA sequencing*

Single-cell suspensions with 1 × $10^5$ cells/mL in PBS (HyClone) were prepared for sequencing. Single-cell suspensions were then loaded onto microfluidic devices, and scRNA-seq libraries were constructed according to the Singleron GEXSCOPE® protocol using the GEXSCOPE® Single-Cell RNA Library Kit (Singleron Biotechnologies). Individual libraries were diluted to 4 nM and pooled for sequencing. Pools were sequenced on an Illumina NovaSeq with 150 bp paired-end reads. Raw reads were processed to generate gene expression profiles using an internal pipeline. Briefly, after filtering Read one without poly-T tails, the cell barcode and UMI were extracted. Adapters and poly-A tails were trimmed (fastp V1) before aligning Read two to GRCh38 with Ensemble version 92 gene annotation (fastp v2.5.3a and featureCounts 1.6.2) [14]. Reads with the same cell barcode, UMI and gene were grouped together to calculate the number of UMIs per gene per cell. The UMI count tables of each cellular barcode were used for further analysis. Single-cell analysis was conducted using Seurat4 [15], and the FindIntegrationAnchors function was used to integrate the datasets, CCA was used as a reduction method during the integration, and the top 20 dimensions were selected for integration. Gene ontology (GO) enrichment analysis was performed using http://geneontology.org and Metascape [16]. Slingshot was used to reconstruct the fibrotic differentiation trajectories [17]. A connectivity map was constructed according to a previous ligand-receptor dataset [18] using CellChat [19].

#### *snATAC-seq*

Was conducted using the 10X Genomics Chromium Single Cell ATAC platform by extracting nuclei from three IUA and three normal endometrial tissues. The sequencing library was sequenced on an Illumina NovaSeq with 150 bp paired-end reads. Raw reads were aligned to GRCh38 using the Cell Ranger-ATAC pipeline. We inferred, filtered potential doublets, conducted quality control and analyzed the snATAC-seq data using the ArchR package [20]. As quality control, the minimum numeric transcription start site (TSS) enrichment score required for a cell to pass filtering for use in downstream analyses was set as 4. The minimum number of mapped ATAC-seq fragments required per cell to pass filtering for use in downstream analyses was set as 1000. The addDoubletScores function was used to filter the doublets: The number of cells neighboring a simulated doublet to be considered as putative doublets was set as 10.

#### *Visium V2 spatial transcriptomic analysis*

Three normal and four IUA endometrial samples fixed in paraffin wax from the pathology department of the Fourth Affiliated Hospital (Ethics Approval Number: K2021113) were used for Visium V2 spatial transcriptomic analysis. Appropriately sized sections were generated for the Visium Spatial slides. The Visium Spatial Tissue Optimization Slide kit was then used to determine the optimal time for permeabilization by generating fluorescently labeled complementary deoxyribonucleic acid (cDNA) tissue prints. The permeabilization process was determined by the time of tissue optimization. The first strand of cDNA was synthesized via reverse transcription and the second strand of cDNA was synthesized via PCR. The cDNA was then denatured, causing the second strand of cDNA to dissociate from the slide. Spatially barcoded, full-length cDNA is amplified via PCR to generate sufficient mass for library construction. The Visium Spatial protocol produces Illumina-ready sequencing libraries. Finally, an Illumina sequencing platform was utilized for high-throughput sequencing using the dual-end sequencing mode. Seurat V4 package and SpaGene package [21] were used for the subsequent spatial transcriptomic data analysis.

### Cell culture, gene and protein expression analysis

#### *Endometrial stromal cell culture*

Fresh normal endometrial tissues were cut into pieces and digested with type I collagenase (0.2%, Sigma) for 1 h at 37 °C. Dissociated cells were then strained through 100 μm and 40 μm strainers respectively and incubated in Dulbecco's Modified Eagle Medium (DMEM)/

F12 containing 10% fetal bovine serum (FBS) and 1% penicillin-streptomycin.

#### *Cytokine treatment*

Normal endometrial stromal cells in passage2 or passage3 were obtained and seeded into 6-well plates at a density of 1 × 105 cells per well. After 24 h incubation, cells were treated with 1% FBS medium for 8 h and then treated with the low-serum medium containing 700ng/mL SPP1 (Peprotech, 120 – 35) or 300ng/mL Galectin-9 (Novoprotein, CR37) cytokines for 48 h, and RNA was collected for RT-qPCR.

#### *Reverse transcription (RT) and real-time PCR*

Reverse transcription (RT) and real-time PCR were performed using an RT kit (Vazyme, R233) and SYBR qPCR kit (Vazyme, Q711-02) according to the protocol of the manufacturer's protocol. The specific primer sequences were β-actin: forward: 5'- AAAGCGGCTGTTAGTCACTGG-3'; reverse: 5'- CGAGTCATTGCATACTGTCCAT-3'. Col1a1 forward: 5'- CGATGGATTCCAGTTCGAGT-3'; reverse: 5'- TTTTGAGGGGGTTCAGTTTG-3'. All the samples were normalized to the internal control, and the fold changes were evaluated using the 2-△△CT method.

#### *Western blot*

Following the reagent instructions, total protein samples were isolated from endometrial stromal cells under different induction conditions using the RIPA lysis buffer. The BCA Protein Assay Kit (Solarbio, Beijing, China) was used to measure the protein concentration. Samples containing 40 μg of protein were separated on a 10% SDS-PAGE gel and transferred to a polyvinylidene fluoride membrane (PVDF, Merck Millipore, 0.45 μm). After blocking the PVDF membrane with protein-free rapid blocking solution (Epizyme Biomedical, Shanghai, China), it was incubated overnight at 4 °C with 1:1000 diluted Rabbit anti-ACTA2 Polyclonal Antibody (Biyotime, AF0048), or with 1:2000 diluted Anti-GAPDH mouse monoclonal antibody (Proteintech, 60004-1-Ig). After washing with TBST, the membrane was incubated with 1:5000 diluted horseradish peroxidase-conjugated anti-mouse IgG (Cell Signaling, 7076) or anti-rabbit IgG secondary antibodies (Cell Signaling, 7074). The generated signal was acquired using a protein imaging system (ChemiDoc Touch; Bio-Rad, Hercules, CA, USA). Protein expression levels were quantified using Imagelab6.0 software and normalized to the loading control, GAPDH.

#### *Bulk RNA-seq*

Total RNA of cultured stromal cells was extracted using TRIzol reagent kit (Invitrogen, Carlsbad, CA, USA) according to the manufacturer's protocol. After quality assessment, eukaryotic mRNA was enriched using Oligo(dT) beads. WI, USA). The enriched mRNA was then fragmented into short fragments using fragmentation buffer and reverse transcribed into cDNA by using the NEBNext Ultra RNA Library Prep Kit for Illumina (NEB #7530, New England Biolabs, Ipswich, MA, USA). RNA chains were then degraded using RNase H. And the second strand of cDNA was synthesized using DNA polymerase I. The purified double-stranded cDNA fragments were subjected to end repair, A-tailing addition, and Illumina sequencing adapter ligation. The ligation reaction product was purified using the AMPure XP Beads (1.0X) and amplified by polymerase chain reaction (PCR). The resulting cDNA library was sequenced using an Illumina NovaSeq 6000 by Gene Denovo Biotechnology Co. (Guangzhou, China).

### IUA animal model

IUA animal model was established as previous method [22]. All animal experiments were approved by the Ethics Committee of Zhejiang University (approval no. ZJU20230011). 7–8 weeks-old female Sprague-Dawley rats were raised in SPF (Specific Pathogen-Free) conditions (22–24 °C, 12 h light/dark cycle) with free access to food and water. They were selected as animal models after a regular estrus cycle was achieved by vaginal smear. After adequate anesthesia was established, a 2 mm transverse incision was made in the middle section of the uterus. The uterus at the incision was turned over with tweezers to cover the inner uterus and extend the length of the uterine intussusception. The endometrial stromal layer was carefully torn off using pointed tweezers. Then, 0.1 mL lipopolysaccharide solution containing 10 mg/L was injected into the uterine cavity at the site where the endometrium was torn off to complete the modeling of uterine cavity adhesion. After 15 days, they were anesthetized with 1% (v/w) pentobarbital and euthanized by $CO_2$ asphyxiation, rat uterine samples were collected for further examination.

### Histology and immunofluorescence

#### *Immunofluorescence staining*

Human endometrial tissues embedded in paraffin were sectioned to a 10 μm thickness. Then, immunofluorescence (IF) staining was carried out using the following protocol: Paraffin sections were subjected to rehydration and antigen retrieval procedures, followed by three consecutive rinses with phosphate-buffered saline (PBS). The sections were then blocked with a 1% bovine serum albumin (BSA) solution for 1 h, after which they were incubated with primary antibodies at 4 °C overnight. The primary antibodies utilized included mouse anti-human CD68 (BioLegend, 333802), rabbit anti-human CD206 (Abcam, ab64693), mouse anti-human CD31 (HuaBio,

M1511-8), rabbit anti-human ACTA2 (Beyotime Biotech, AF0048), rabbit anti-human KRT8 + 18 (Beyotime Biotech, AF1618), and mouse anti-human ACTA2 (Beyotime Biotech, AA132), were used. Secondary antibodies: goat anti-rabbit Alexa Fluor 488 (Invitrogen, A11008), donkey anti-mouse Alexa Fluor 546 (Invitrogen, A10036) and DAPI was applied to stain cell nuclei, with fluorescent secondary antibodies used to visualize the binding signals of the corresponding primary antibodies. All experimental steps were executed in strict accordance with the manufacturers' recommended protocols.

#### *Masson's trichrome staining*

Paraffin-embedded endometrial samples from human IUA endometrial samples and rat uterus samples were cut into 10-μm-thick sections. These sections were subsequently processed for rehydration and antigen retrieval, rinsed thoroughly with PBS three times, and then subjected to Masson's trichrome staining with a commercial staining kit (Solarbio, G1340). All procedures were performed according to the manufacturer's instructions. The fibrotic regions of individual samples were automatically identified and quantified by means of the count and measure objects plugin integrated in Image-Pro Plus 6.0 software.

### Statistical analysis

The quantitative enrichment of $ACTA2^{+}KRT8^{+}$ myogenic epithelial cells, $ACTA2^{+}$ $CD31^{+}$ myogenic endothelial cells in immunofluorescence staining images of normal and IUA endometrium were compared using Wilcoxon signed-rank test in PRISM 8.0. The comparison of $CD68^{+}CD206^{+}$ macrophages in immunofluorescence staining images of normal and IUA endometrium were conducted via unpaired t-test in PRISM 8.0 software, where a *P*-value of less than 0.05 was defined as statistically significant. The comparison of macrophage proportions between normal and IUA endometrium in the single cell data was conducted via unpaired t-test in PRISM 8.0 software, where a *P*-value of less than 0.05 was defined as statistically significant. Correlation analysis between macrophage number and age, AFS score and fibrotic area ratio of IUA endometrial samples was conducted using Pearson correlation coefficient analysis in PRISM 8.0, with *P*-values less than 0.05 considered statistically significant. Unpaired t-test was used to compare the relative *COL1A1* and *ACTA2* mRNA expression levels in endometrial stromal cells treated with or without SPP1 and Galectin9 recombinant proteins, with *P*-values less than 0.05 considered statistically significant. The comparison of ACTA2 protein levels in endometrial stromal cells treated with or without SPP1 was also performed via unpaired t-test in PRISM 8.0 software, where a *P*-value of less than 0.05 was defined as statistically significant. The comparison of the fibrotic area ratio in normal and IUA rat endometrium was conducted via unpaired t-test in PRISM 8.0 software, where a *P*-value of less than 0.05 was defined as statistically significant. The comparison of the expression level of epithelial-mesenchymal transition (EMT) markers was first conducted by using an ANOVA test to determine significant differences in gene expression levels among different subgroups of cells. If the ANOVA test showed significant differences, Turkey HSD test was then used for pairwise comparisons to determine the significance of differences between subgroups.

## Results

### Single-cell multi-omic atlas of human IUA and normal endometrium

To gain a systematic understanding of the underlying cellular and molecular mechanisms of IUA pathogenesis, we profiled human endometrial cells from nine IUA endometriala samples and three normal endometrial samples using a scRNA-seq platform. We also integrated these data with scRNA-seq data from six normal human endometrium samples collected from two published datasets, including the ArrayExpress datasets under accession numbers E-MTAB-10287 and NCBI's Gene Expression Omnibus datasets with accession code GSE111976 [23, 24]. Thus, single-cell RNA-seq data from 9 IUA and 9 normal endometrial samples were included for the analysis of IUA pathogenesis. All samples were confirmed to be in the proliferative phase to avoid the physiological interference from the menstrual cycle. The sample information for the three datasets (our study, E-MTAB-10287 and GSE111976) is shown in Table S1 (Additional file 1). All the integrated single-cell RNA-seq data from 9 IUA and 9 normal endometrial samples were subjected to quality control, data integration, cell type identification and clustering analysis by using the Seurat V4 R package [15]. After computational quality control by filtering the data based on the number of counts (nCount_RNA < 40000) and number of features (nFeature_RNA < 6000), 57,835 single cells from normal endometrium and 31,842 single cells from IUA endometrium were retained for the following analysis (Additional file 1: Table S2). We then selected highly variable genes from the 1–8 principal component (PC) to perform downstream clustering on all cells. All cells from 9 normal and 9 IUA samples could be clustered into five main clusters, which could be visualized using Uniform Manifold Approximation and Projection (UMAP) (Fig. 1A). Both IUA and normal endometria contained the five main cell clusters (Fig. 1B). All the main cell clusters were homogeneously distributed in the three datasets (our study, E-MTAB-10287 and GSE111976) (Fig. 1C), indicating the successful integration of the datasets and removal of batch effects. Each main cluster highly expressed its specific marker gene

set (Fig. 1D and E). According to the marker gene sets of each main cluster, cell clusters with high expression of *COL1A1* and *ECM1* were annotated as stroma cells, cell clusters with high expression of *CLDN5* and *VWF* were annotated as endothelia cells, cell clusters with high expression of *EPCAM*, *KRT18* and *KRT8* were annotated as epithelia cells, cell clusters with high expression of *ACTA2* were annotated as muscle cells, and cell clusters with high expression of *PTPRC*, *CD68* and *CD3E* were annotated as immune cells (Fig. 1D). All cells from the 9 normal and 9 IUA samples could also be further clustered into 27 subpopulations according to the specific marker gene sets (Additional file 3: Fig. S1A-S1C).

We then performed snATAC-seq to confirm and validate the cell types identified in the scRNA-seq analysis. The snATAC-seq data of three IUA patients and three normal endometrial tissues were profiled (Fig. 1F and I). We aligned the sequencing reads to GRCh38 with ensemble version 92 gene annotation and analyzed the snATAC-seq data by using the ArchR package [20]. After quality control, we obtained and profiled 7332 and 8489 single nucleus ATAC-seq data from IUA patients and normal endometrial tissues, respectively. Similar to the single cell data, all single nuclei data from both IUA and normal endometrial samples could be clustered into five main cell types according to their unique gene scores (Fig. 1F). Both IUA and normal endometria contained the five main cell clusters in the ATAC-seq data (Fig. 1G). The heatmap shows the specific gene activity of the five main cell types by snATAC-seq (Fig. 1H). The normalized chromatin accessibility profiles showed that each main cell type had a highly specific peak at its canonical marker gene position: for example, endothelia cells showed a high peak of *CLDN5*, epithelia cells showed *a* high peak of *EPCAM*, immune cells showed a high peak of *PTPRC*, smooth muscle cells showed a high peak of *ACTA2* and stroma cells showed a high peak of *COL1A1* (Fig. 1I). By further subgroup analysis, 13 subpopulations identical to those in the scRNA-seq data could also be detected in the snATAC-seq data (Additional file 3: Fig. S1D-S1E). The results showed that the cell types identified by snATAC-seq analysis were consistent with most of those identified by scRNA-seq analysis.

### Identification of heterogeneous fibrotic cell populations in human IUA by scRNA-seq

Previous studies have shown that fibrotic cells are the driving factors of tissue fibrosis [10] and myofibroblasts are considered the only fibrotic cells during the fibrosis process of IUA [25]. Importantly, in addition to fibrotic myofibroblasts in the stromal cell clusters of IUA, we also investigated the potential fibrotic cell populations in the epithelial and endothelial cell clusters of human IUA.

First, we analyzed stroma cell data by clustering them into subpopulations and comparing the cellular and molecular pathological changes between IUA and normal endometrium. As visualized in the UMAP (Fig. 2A and B), all stromal cells could be grouped into four sub-clusters according to their unique marker gene sets (Fig. 2C and D). The cell cluster expressing high levels of *SFRP4* and *IGF1* was annotated as SFRP4_stroma [26], the cell cluster expressing high levels of *NFKBIA* was annotated as inflammatory_stroma, the cell cluster expressing high levels of *ACTA2*, *ADIRF* and *PDGFRB* was annotated as myogenic_stroma (or myofibroblast), and the cell cluster expressing high levels of *MKI67* was annotated as proliferative_stroma (Fig. 2D). According to the cell proportion of the four stromal subpopulations in each donor of IUA and normal endometrium, myofibroblasts showed increased an proportion in IUA samples, while inflammatory_stroma had a decreased cell proportion in IUA samples (Fig. 2E). Since myofibroblasts are considered the main fibrotic cells during the fibrosis process of IUA [25], we characterized the molecular characteristics of myofibroblasts in IUA at the single-cell level. Gene ontology (GO) analysis showed that myofibroblasts were significantly enriched in GO terms such as myofibril assembly, extracellular matrix organization, tissue remodeling and negative regulation of angiogenesis (Additional file 2: Table S4).

We also identified fibrotic epithelial cells by clustering all epithelial cells into subpopulations and comparing the pathological changes between IUA and normal endometrium. As visualized in UMAP (Fig. 2F and G), all epithelial cells could be grouped into seven sub-clusters according to their unique marker gene sets (Fig. 2H). Cell clusters with high expression of *SCGB1D2* and *SCGB2A1* were annotated as secretory_epi; cell clusters highly expressing *MKI67* were annotated as proliferative_epi; cell clusters highly expressing *ACTA2* were annotated as myogenic_epi; cell clusters with high expression of *SOX9* were annotated as intermediate_epi (Reason for defining intermediate_epi: From the pseudotime analysis, this cell cluster is in an intermediate state towards the differentiation of four lineages, all other lineages would pass through this cell cluster, hence it is defined as intermediate_epi) (Fig. 3F); cell clusters with high expression of *CXCL2* and *CXCL8* were annotated as inflammatory_epi; cell clusters highly expressing *NEAT1* were annotated as healing_epi (Reason for defining healing_epi: This cell cluster contains a large number of terms related to wound healing in its GO terms, therefore we define this cell cluster as healing_epi); and cell clusters highly expressing *TPPP3* were annotated as ciliated_epi. (Fig. 2I). GO analysis of myogenic_epi specific markers showed that the GO terms of elastic fiber assembly,

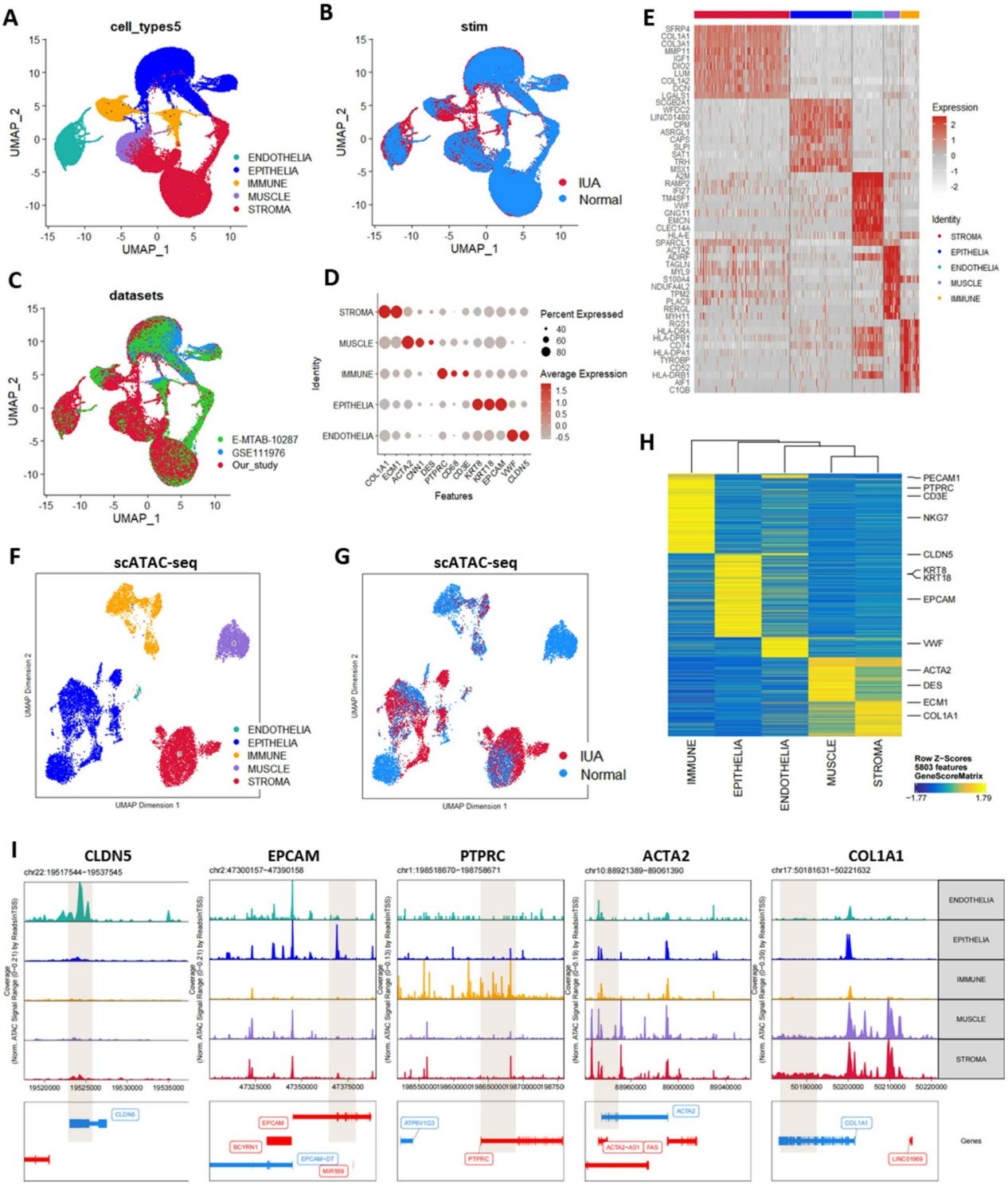


**Fig. 1** (See legend on next page.)

(See figure on previous page.)

**Fig. 1** Single cell multiomic atlas of human intrauterine adhesion (IUA) and normal endometrium. **A** UMAP plot of all collected cells colored by 5 main cell types of the IUA and normal endometrium by single cell RNA-seq (scRNA-seq). **B** UMAP plot of all collected cells colored by groups (intrauterine adhesion (IUA) and normal groups) in scRNA-seq. **C** UMAP plot of all collected cells colored by different datasets (scRNA-seq data named E-MTAB-10287 were collected from published ArrayExpress datasets under accession numbers E-MTAB-10287; scRNA-seq data named GSE111976 were collected from published NCBI's Gene Expression Omnibus datasets (series accession code GSE111976)). **D** Dot plot showing specific marker genes for each main cell type (COL1A1, ECM1 for stroma cells; ACTA2 for smooth muscle cells; PTPRC, CD68, CD3E for immune cells; EPCAM, KRT8, KRT18 for epithelial cell; CLDN5, VWF for endothelial cells). **E** Heatmap showing specific gene expression of the 5 main cell types by scRNA-seq. **F** snATAC-seq UMAP plot of all collected cells colored by 5 main cell types of the IUA and normal endometrium. **G** UMAP plot all collected cells colored by groups of IUA and normal endometrium in snATAC-seq. **H** Heatmap showing specific gene activity of the 5 main cell types by scATAC-seq. **I** Normalized chromatin accessibility profiles of canonical marker genes for 5 main cell types (CLDN5 for endothelial cells; EPCAM for epithelial cell; PTPRC for immune cells; ACTA2 for smooth muscle cells; COL1A1 for stroma cells). The chromosome position of each gene is shown below

collagen fibril organization, fibroblast proliferation, and cellular response to transforming growth factor beta stimulus were significantly enriched in this fibrotic epithelial cell population (Additional file 2: Table S4), indicating the fibrotic characteristics of this myogenic_epi population. The proportion of epithelial subpopulations showed a high proportion of myogenic_epi in two out of nine IUA endometria (Fig. 2J). Considering human differences, we collected more samples for protein level validation to confirm whether there is an enrichment of this fibrotic epithelial population in IUA endometrial tissue. An additional 11 normal endometrial samples and 39 IUA samples were included. Patients' clinical information is shown in Table S3 (Additional file 1). Consistent with the single-cell level results, Immunofluorescence (IF) staining results showed that not every IUA sample had a significantly high level of α-SMA+KRT8 + double-positive cells (Fig. 2L). However, the overall results of the protein level validation confirmed the high enrichment of the myogenic epithelium in the endometrium of IUA (Fig. 2K and L).

We also revealed fibrotic endothelial cells by clustering all endothelial cells into subpopulations and comparing their cellular and molecular pathological changes between IUA and normal endometria. As visualized in the UMAP (Fig. 2M and N), all endothelial cells could be grouped into seven sub-clusters according to their unique marker gene sets (Fig. 2O), Cell clusters highly expressing *THY1* and *COL4A1* were annotated as THY1_endo; cell clusters highly expressing *SLCO2A1* were annotated as SLCO2A1_endo; cell clusters highly expressing *MKI67* were annotated as proliferative_endo; cell clusters highly expressing *ACTA2* were annotated as myogenic_endo; cell clusters highly expressing *JAG1* were annotated as JAG1_endo; cell clusters highly expressing *NFKBIA* were annotated as inflammatory_endo; and cell clusters highly expressing *CLU* were annotated as CLU_endo (Fig. 2P). GO analysis of myogenic_endo-specific markers showed that GO terms of elastic fiber assembly, collagen fibril organization, myofibril assembly, muscle contraction, and cell adhesion were significantly enriched in this endothelial fibrotic cell population (Additional file 2: Table S4). The proportion of endothelial subpopulations showed the existence of myogenic_endo in both IUA and normal endometrium, but a high proportion of myogenic_endo in normal endometrium (Fig. 2Q). On the contrary, IF staining of α-SMA+CD31 + endothelial cells revealed highly enriched myogenic endothelia in the IUA endometrium (Fig. 2R and S).

Thus, we not only confirmed the fibrotic myofibroblast cluster in the IUA endometrium, but also identified diverse fibrotic cell populations in the epithelium and endothelium of the human IUA endometrium. We also characterized the shared molecular features of these three fibrotic cell types, which were enriched with the same extracellular matrix (ECM) organization-related GO terms, indicating their direct involvement in the production and aggregation of extracellular matrix. As tissue fibrosis is defined by the excessive accumulation of ECM components [10], although the enrichment of myogenic_endo in IUA tissue is indeterminate, the high enrichment of myogenic_stroma and myogenic_epi in IUA tissues implies a direct contribution of these two fibrotic cell populations to the pathogenesis of human IUA.

### Differentiation trajectory of fibrotic cell populations in human IUA by scRNA-seq and scATAC-seq

Next, we aimed to reconstruct and characterize the fibrotic differentiation trajectories of multiple fibrotic cell lineages during human endometrial fibrosis. Slingshot was used to reconstruct the fibrotic differentiation trajectories of myofibroblasts, myogenic epithelial cells and myogenic endothelial cells, respectively (Fig. 3) [27].

For the stromal cell differentiation, the myogenic_stroma originated from the proliferative_stroma and went through the lineage1 branch of the trajectory, finally differentiating into myogenic_stroma (Fig. 3A). According to the molecular characteristics of pseudotime, the expression level of *ACTA2* significantly increased during the differentiation process of myogenic_stroma (Fig. 3B). Transcription factor (TF) activity analysis by using the SCENIC package identified myogenic_stroma-specific TFs (Fig. 3C). Among them, it was known that GATA2, STAT6, FOSL2, ETS1 and MEF2C are known to be involved in the development of liver [28, 29], renal [30] or dermal fibrosis [31]. Notably, the snATAC-seq results

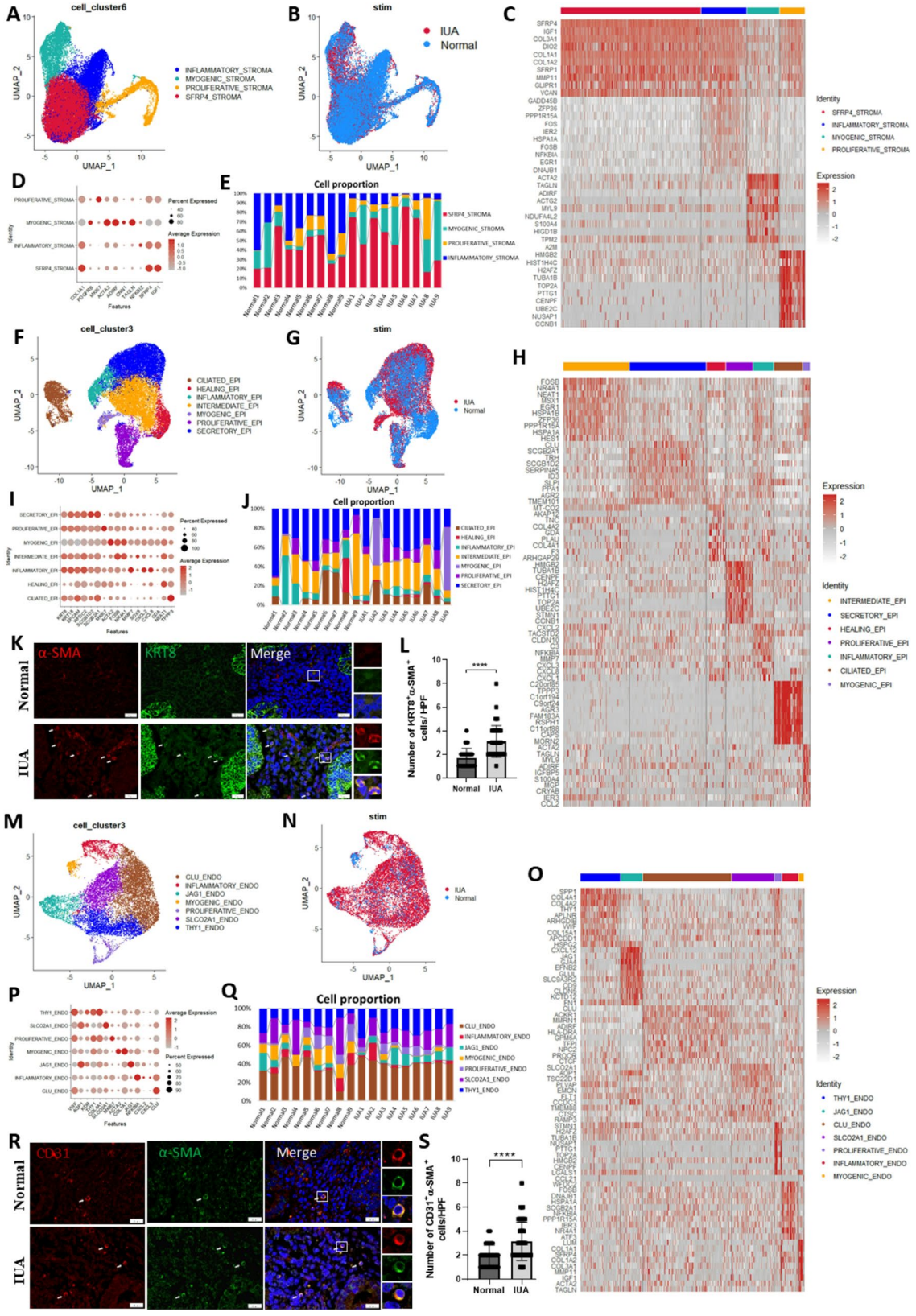


**Fig. 2** (See legend on next page.)

(See figure on previous page.)

**Fig. 2** Identification of heterogenous fibrotic cell populations in human IUA by scRNA-seq. **A** UMAP plot of all stromal cells colored by 4 subset cluster identity of IUA and normal endometrium in scRNA-seq. **B** UMAP plot of all stromal cells colored by groups (IUA and normal groups) in scRNA-seq. **C** Heatmap showing specifically expressed gene signature of the 4 stromal subpopulation cell types of IUA and normal endometrium. **D** Dot plot showing specific marker genes for each stromal subpopulation. **E** Cell proportion of 4 stromal subpopulation in IUA and normal endometrium by scRNA-seq. **F** UMAP plot of all epithelial cells colored by 7 subset cluster identity of IUA and normal endometrium in scRNA-seq **G**. UMAP plot of all epithelial cells colored by groups (IUA and normal groups) in scRNA-seq. **H** Heatmap showing specifically expressed gene signature of the 7 epithelial subpopulation cell types of IUA and normal endometrium. **I** Dot plot showing specific marker genes for each epithelial subpopulation. **J** Cell proportion of 7 epithelial subpopulation in IUA and normal endometrium by scRNA-seq. **K** Representative Immunofluorescence (IF) staining image of KRT8+α-SMA+ myogenic_epithelia in normal and IUA endometrium, Scale bar=20 μm; the magnification image with split color of the white box area showed on the right. **L** Quantitative comparison of the number of KRT8+α-SMA+ myogenic_epithelia cells per high power field (HPF) from IF images in normal (n=11) and IUA endometrium (n=39). ****, P value<0.0001. **M** UMAP plot of all endothelial cells colored by 7 subset cluster identity of IUA and normal endometrium in scRNA-seq. **N** UMAP plot of all endothelial cells colored by groups (IUA and normal groups) in scRNA-seq. **O** Heatmap showing specifically expressed gene signature of the 7 endothelial subpopulation cell types of IUA and normal endometrium. **P** Dot plot showing specific marker genes for each endothelial subpopulation. **Q** Cell proportion of 7 endothelial subpopulation in IUA and normal endometrium by scRNA-seq. **R** Representative Immunofluorescence (IF) staining image of CD31+α-SMA+ myogenic_endothelia in normal and IUA endometrium, Scale bar=20 μm; the magnification image with split color of the white box area showed on the right. **S** Quantified comparison of the number of CD31+α-SMA+ myogenic_endothelia cells per HPF from IF images in normal (n=11) and IUA endometrium (n=39). ****, P value<0.0001.

also detected upregulated chromatin accessibility profiles of TFs (*GATA2*) in myogenic_stroma. The results of immunostaining proved that GATA2 had a significantly higher expression level in stromal cells in IUA endometrium (Fig. 3E, Additional file 3: Fig. S2A). It is worth noting that the results of snATAC-seq also detected upregulated chromatin accessibility profiles of *SMAD1* in Myogenic_stroma. SMAD1 is involved in TGF-β1/ALK1/Smad1 pathway, which is proved to have important role in fibrosis development in multiple tissues [32].

For the epithelial differentiation, the myogenic_epi originated from the proliferative_epi, passed through the intermediate_epi and finally differentiated into myogenic_epi (Lineage2) (Fig. 3F). The molecular characteristics over pseudotime proved the increased expression level of *ACTA2* in the differentiation process of myogenic_epi (Lineage2), increased expression level of *TPPP3* in the differentiation process of ciliated_epi (Lineage1) and increased expression level of *PEAP* in the differentiation process of secretory_epi (Lineage3) (Fig. 3G). The transcription factor (TFs) activity analysis identified myogenic_epi-specific TFs (Fig. 3H), including *CEBPD*, *JUN*, *NR3C1*, *EOMES*, *ZEB1*, *HOXD10*, *IRF2*, *RFXAP* and *TWIST2*. The results of snATAC-seq validated the upregulated chromatin accessibility profiles of EMT and fibrosis related TFs, including *TWIST2* [33] and *SMAD3* [34, 35] in myogenic_epi compared with other epithelial subpopulations (Fig. 3I). The results of immunostaining confirmed that TWIST2 had a significantly higher expression level in epithelial cells in IUA endometrium (Fig. 3J, Additional file 3: Fig. S2B). Epithelial-mesenchymal transition (EMT) is involved in IUA progression [36, 37]. In this study, we identified myogenic_epi, which is highly enriched in the IUA endometrium and has an upregulated TF of *ZEB1*, as ZEB1 is known to be an EMT master regulator [38]. We compared the expression level of epithelial markers (*EPCAM* and *CDH1*) and mesenchymal markers (*ACTA2* and *COL1A1*) in 7 epithelial subpopulations. The results showed that the myogenic_epi populations had significantly downregulated epithelial markers and upregulated mesenchymal markers (Additional file 3: Fig. S3), which confirmed the EMT characteristics of myogenic_epi in the fibrosis process of human IUA.

For the endothelial differentiation, the myogenic_endo cells originated from the proliferative endothelial cells, went through the THY1_endo and finally differentiated into myogenic_endo (Fig. 3K). The molecular characteristics over pseudotime also proved the increased expression level of *ACTA2* in the differentiation process of myogenic_endo (Lineage3) (Fig. 3L). The results of scRNA-seq identified the myogenic_endo-specific TFs, including *DBP* and *ZNF581* (Fig. 3M). Due to the limited number of endothelial cells detected by snATAC-seq and there were no subpopulations in endothelial cells (Fig. 1F and Additional file 3: Fig. S1D), we were unable to validate the chromatin accessibility profiles of myogenic_endo-specific TFs at snATAC levels.

Thus, we reconstructed and characterized the fibrotic differentiation trajectories and molecular regulators of three fibrotic cell lineages during human endometrial fibrosis. And we have demonstrated fibrosis related TFs specific to myogenic_stroma and myogenic_epi subgroups, which may provide new molecular targets for the development of therapeutic treatments for IUA.

### The pro-fibrotic immune microenvironment of human IUA

The role of the disease microenvironment especially the immune microenvironment has been a research hotspot in the process of disease development [10]. Therefore, we reconstructed the immune microenvironment of IUA and normal endometrium by clustering immune cells into subpopulations and comparing their cellular and molecular pathological changes. As visualized in the UMAP (Fig. 4A and B), all immune cells could be grouped into eight sub-clusters according to their unique marker gene

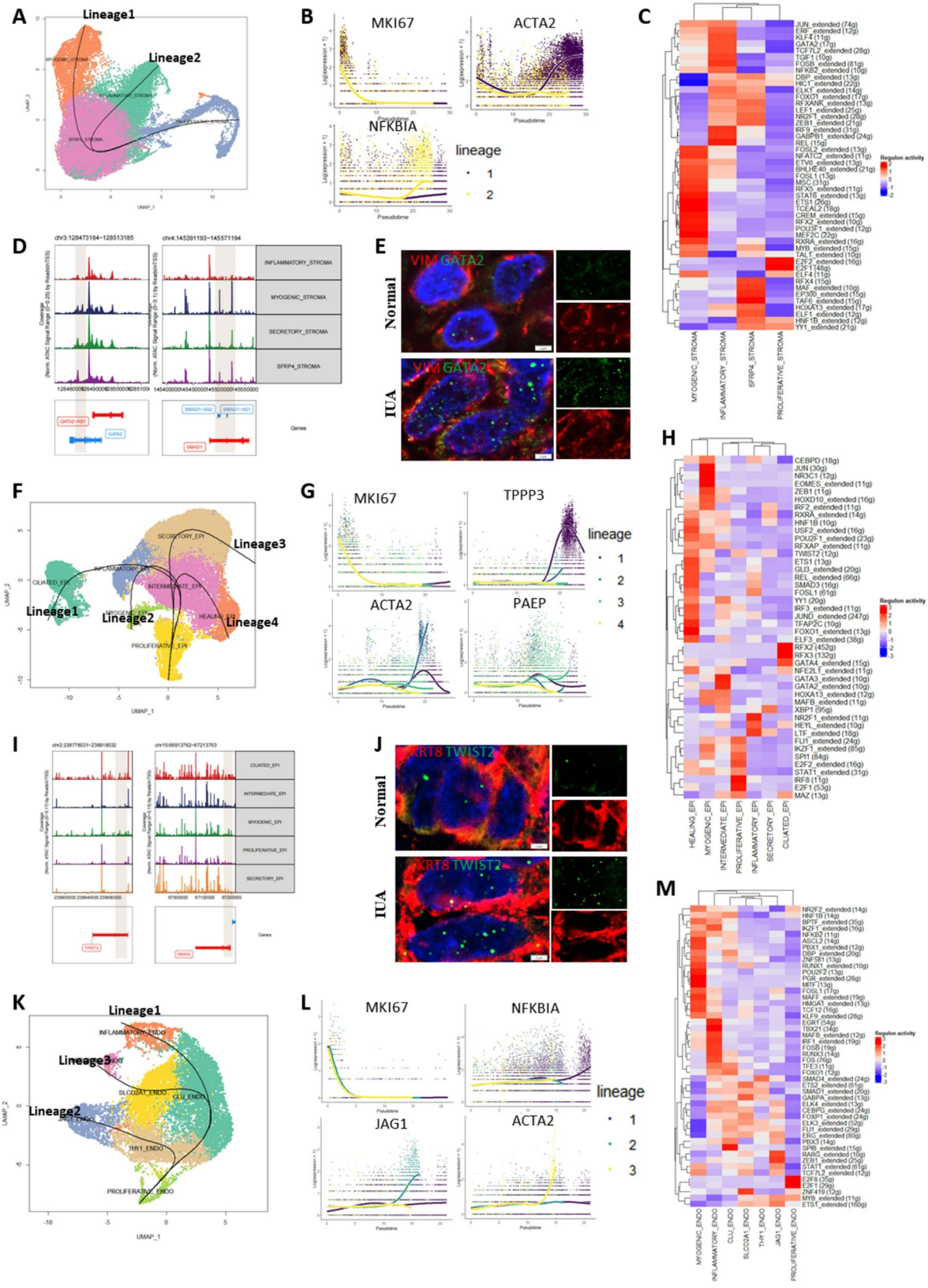


**Fig. 3** (See legend on next page.)

(See figure on previous page.)

**Fig. 3** The differentiation trajectory of fibrotic cell populations in human IUA by scRNA-seq and scATAC-seq. **A** UMAP plot of pseudo-space ordering of all the stromal sub-clusters by scRNA-seq. **B** Lineage specific gene expression pattern along pseudo-time from differentiation trajectory of stromal cells. **C** Heatmap of transcription factors (TFs) activity in each stromal cell subpopulation by scRNA-seq. **D** Normalized chromatin accessibility profiles of TFs upregulated in Myogenic_stroma; The chromosome position of each gene shown below. **E** Representative image of IF staining of VIM and GATA2 in normal and IUA endometrium, Scale bar=2 μm. **F** UMAP plot of Pseudo-space ordering of all the epithelial sub-clusters by scRNA-seq. **G** Lineage specific gene expression pattern along Pseudo-time from differentiation trajectory of epithelial cells. **H** Heatmap of transcription factors (TFs) activity in each epithelial cell subpopulation. **I** Normalized chromatin accessibility profiles of TFs upregulated in Myogenic_epi; The chromosome position of each gene shown below. **J** Representative image of IF staining of KRT8 and TWIST2 in normal and IUA endometrium, Scale bar=2 μm. **K** UMAP plot of Pseudo-space ordering of all the endothelial sub-clusters by scRNA-seq. **L** Lineage specific gene expression pattern along Pseudo-time from differentiation trajectory of endothelial cells. **M** Heatmap of transcription factors (TFs) activity in each endothelial cell subpopulation

sets (Fig. 4C). Cell subclusters expressing high levels of *GNLY* were annotated as NK cells (NK_1 and NK_2). Cell subclusters expressing high levels of *CD3D* and negative expression of *GNLY* were annotated as T cells (T_cells_1 and T_cells_2), cell subclusters expressing high levels of *CD68*, *IL1B* and *MRC1* were annotated as macrophages, cell subclusters expressing high levels of *CD1C* were annotated as DC (dendritic cell) cells, cell subclusters expressing high levels of *JCHAIN* were annotated as B cells (B_cells_1 and B_cells_2) (Fig. 4D). According to the proportion of each immune sub-population in each donor from IUA and normal endometrium, macrophages were significantly highly enriched in IUA endometrium, while the T_cells_1 and NK_1 cell populations were decreased in IUA samples (Fig. 4E and F). As the macrophages showed M2-like macrophage characteristics with positive expression of *MRC1* (namely *CD206*) (Fig. 4D), we performed IF staining for CD68 and CD206 for macrophage identification. The results of IF staining further confirmed that macrophages were highly enriched in the IUA endometria compared with the normal endometria (Fig. 4G and H).

In order to further understand a clinical insight of macrophage in IUA, we conducted correlation analysis between the number of macrophages and clinical characteristics such as age, AFS score (Evaluation criteria from The American Fertility Society) and fibrotic area ratio in 39 clinical samples of IUA. The results showed that the number of macrophages in IUA tissues was significantly positively correlated with the AFS score and fibrotic area ratio in IUA tissues (Fig. 4J and K), indicating that the more severe the intrauterine adhesion, the greater the macrophage accumulation. These results demonstrated a highly positive correlation between the macrophage-enriched microenvironment and pathological changes in IUA.

### The multi-lineage interactome in the fibrotic niche of human IUA

Next, in order to further investigate how the pathological immune microenvironment regulates the disease progression in IUA, we conducted a multi-lineage interaction analysis and compared the fibrotic niche between the normal and IUA endometrium by using CellChat. We found a dramatic difference in the interaction niche between normal and IUA endometrium (Fig. 5A and B). When compared with normal endometrium, the macrophages and stroma cell populations in the IUA endometrium showed significantly stronger interaction intensity (Fig. 5A). According to the comparison of information flow between IUA and normal endometrium (Fig. 5B), we found that canonical growth factors known for tissue regeneration and homeostasis (*GDF*, *WNT*, *BMP*, *FGF*, *EGF*, *IGF*) were significantly downregulated in the IUA endometrium. *IL6*, a well-known hallmark for endometrial pregnancy maintenance [39], was also significantly downregulated in the IUA endometrium. However, signals positively correlated with tissue fibrosis, including *GALECTIN*, *MK*, *PTN*, *ANNEXIN*, *SPP1*, *PERIOSTIN*, *COMPLEMENT*, *IL16*, *IL1* and *BAFF*, were upregulated in the IUA endometrium, indicating typical pro-fibrotic features in the microenvironment of IUA tissue.

Given that we had confirmed the potential pro-fibrotic effect of macrophages in IUA (Fig. 4), we wanted to determine how macrophages promote fibrosis. We then analyzed the ligand-receptor interactions between macrophages and the three fibrotic cell lineages. Two ligand-receptor pairs showed stronger interactions between macrophages and the three fibrotic cell lineages: including *SPP1-CD44* and *LGALS9-CD44* (Fig. 5C). Macrophages had higher expression levels of *SPP1* and *LGALS9* (encoding *Galectin9*) in the IUA group than in the normal endometria (Fig. 5D). These results indicate that macrophages in IUA tissue may promote multiple lineage fibrotic changes through SPP1 and LGALS9/Galectin9.

To verify the stronger interaction between *SPP1-CD44* and *LGALS9-CD44* in IUA, we performed Visium V2 spatial transcriptomic analysis on normal and IUA endometrial samples. We confirmed the greater spatial transcriptomic co-localization (blue points) of *LGALS9-CD44* pairs in the IUA endometrium (Fig. 5E). To investigate the role of SPP1 and LGALS9/Galectin9 in fibrosis progression in IUA, we treated the in vitro cultured human endometrial stromal cells with recombinant proteins (SPP1 and Galectin9) and measured the gene expression levels of *ACTA2* and *COL1A1* after treatment. The results showed that both SPP1 and LGALS9/Galectin9 treatment induced significantly high expression

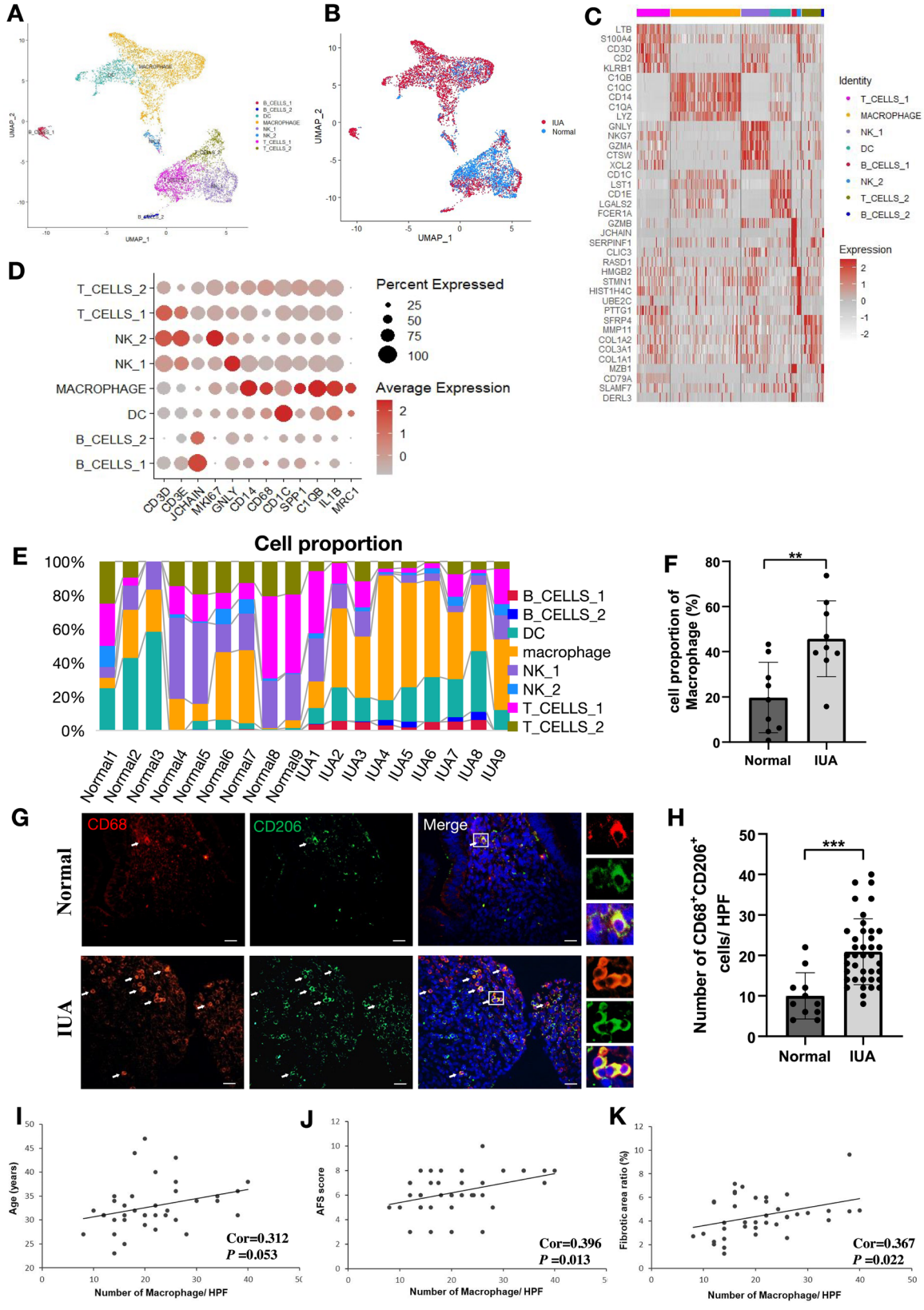


**Fig. 4** (See legend on next page.)

(See figure on previous page.)

**Fig. 4** The pro-fibrotic immune microenvironment of human IUA. **A** UMAP plot of all immune cells colored by 8 subset cluster identity of IUA and normal endometrium in scRNA-seq. **B** UMAP plot of all immune cells colored by groups (IUA and normal groups) in scRNA-seq. **C** Heatmap showing specifically expressed gene signature of the 8 immune subpopulation cell types of IUA and normal endometrium. **D** Dot plot showing specific marker genes for each immune subpopulation. **E** Cell proportion of 8 immune subpopulation in IUA and normal endometrium by scRNA-seq. **F** Quantitative cell proportion of macrophages between normal and IUA endometrium by scRNA-seq, n=9 in each group, **, P value<0.01. **G** Representative IF staining image of CD68+CD206+ macrophage in normal and IUA endometrium, Scale bar=20 μm; the magnification image with split color of the white box area shown on the right. **H** Quantitative comparison of the number of CD68+CD206+ macrophages per HPF from IF images in normal (n=11) and IUA endometrium (n=39). ***, P value<0.001. **I** The scatter plots representing the correlation coefficient between macrophages and age in IUA samples (n=39). **J** The correlation coefficient between macrophages and AFS score in IUA samples (n=39). **K** The correlation coefficient between macrophages and fibrotic area ratio in IUA endometrium (n=39)

levels of fibrosis markers (*ACTA2* and *Col1a1*) (Fig. 5F and G). These results confirmed the pro-fibrotic effect of SPP1 and LGALS9/Galectin9 secreted by macrophages on endometrial cells during IUA progression.

Because SPP1 and LGALS9/Galectin9 act on the same receptor (CD44), we chose one of the ligands (SPP1) for further validation. Western blot analysis confirmed the significantly higher expression level of ACTA2 protein after SPP1 treatment (Fig. 5H). Bulk RNA sequencing analysis of endometrial stromal cells with or without SPP1 treatment was also performed to verify the pro-fibrotic effect of SPP1 (Fig. 5I). Analysis of differentially expressed genes (DEGs) showed that most of DEGs were upregulated in the SPP1 treatment group compared with the control group (Fig. 5J). GO analysis of upregulated DEGs showed that GO terms of extracellular matrix organization, cellular response to transforming growth factor beta stimulus and production were significantly enriched in endometrial stromal cells treated with SPP1 (Fig. 5K). According to the TF analysis, many of the upregulated TFs (*KLF4*, *MEF2C*, *NFATC2*, *ETV6*, *FOSL1*, *ETS1*) induced by SPP1 treatment were myogenic_stroma specific TFs by scRNA-seq analysis (Figs. 3C and 5L), indicating the same phenotype of SPP1 treated stromal cells in vitro with myogenic_stroma cell population identified in vivo. These results proved that SPP1 treatment could indeed induce endometrial stromal cells into fibrotic characterized stromal cells.

### Homology of IUA pathology between human and rat species

To explore the IUA pathology across species, we constructed a rat IUA model according to a previously described method [22]. The results of Masson's trichrome staining confirmed the successful construction of the IUA animal model, with a significant increase in the fibrotic area ratio in the rat IUA group (Additional file 3: Fig. S4A-4B). We then performed scRNA-seq analysis of uterus from the normal and IUA rats. According to the canonical marker genes of cell types, five main clusters were detected in rat normal and IUA uterus, including stroma, muscle cells, immune cells, epithelia and endothelia (Additional file 3: Fig. S4C-4E). Further subgroup analysis of each main cluster was also performed to identify heterogeneous fibrotic cell populations. Consistent with human IUA, three fibrotic cell populations of three lineage were also present in the uterus tissue of rat IUA, including myogenic_stroma, myogenic_epi and myogenic_endo (Additional file 3: Fig. S5A-S5B, S5F-S5G, S5K-S5L). All these three fibrotic cell populations expressed relatively high levels of ACTA2 (Additional file 3: Fig. S5C, S5H, S5M). According to the comparison of cell proportions between rat IUA and normal endometrium, myogenic_stroma and myogenic_epi were highly enriched in the rat IUA uterus (Additional file 3: Fig. S5D, S5I, S5N). The transcription factor (TF) activity analysis identified specific TFs in each myogenic cell population (Additional file 3: Fig. S5E, S5J, S5O). Although the specific TFs in each rat myogenic population were different from those in each human myogenic population, many of the rat myogenic population-specific TFs were pro-fibrotic candidates in various tissues, such as *Creb3l1* in myogenic_stroma, *Jund*, *Nanog*, *Ets1*, *Cebpb* and *Elk3* in myogenic_epi, *Nfatc1*, *Cebpb*, *Creb1*, *Gata6* and *Elk3* in myogenic_endo, indicating the fibrotic characteristics of myogenic populations from these lineages in the rat IUA model.

The immune microenvironment in the rat IUA endometrium was also analyzed by clustering all immune cells into subpopulations and comparing their cellular and molecular changes (Additional file 3: Fig. S6A-S6C). Macrophages were found to be highly enriched in the rat IUA uterus (Additional file 3: Fig. S6D). The expression levels of *Spp1* and *Lgals9*, mainly secreted by macrophages, were also higher in rat IUA than those in normal endometrium (Additional file 3: Fig. S6E). These results in rat IUA were highly consistent with the pathological changes of human IUA, clarifying the homology of pathology between human IUA and the rat IUA model.

## Discussion

Endometrial fibrosis in IUA can cause adverse pregnancy outcomes and even infertility. Here, we demonstrated heterogeneous and novel fibrotic cell lineages in IUA using a comprehensive single cell multi-omics atlas. We revealed the distinct molecular characteristics and their differentiation trajectories of three fibrotic cell lineages in the endometrium of human and rat IUA. The myogenic

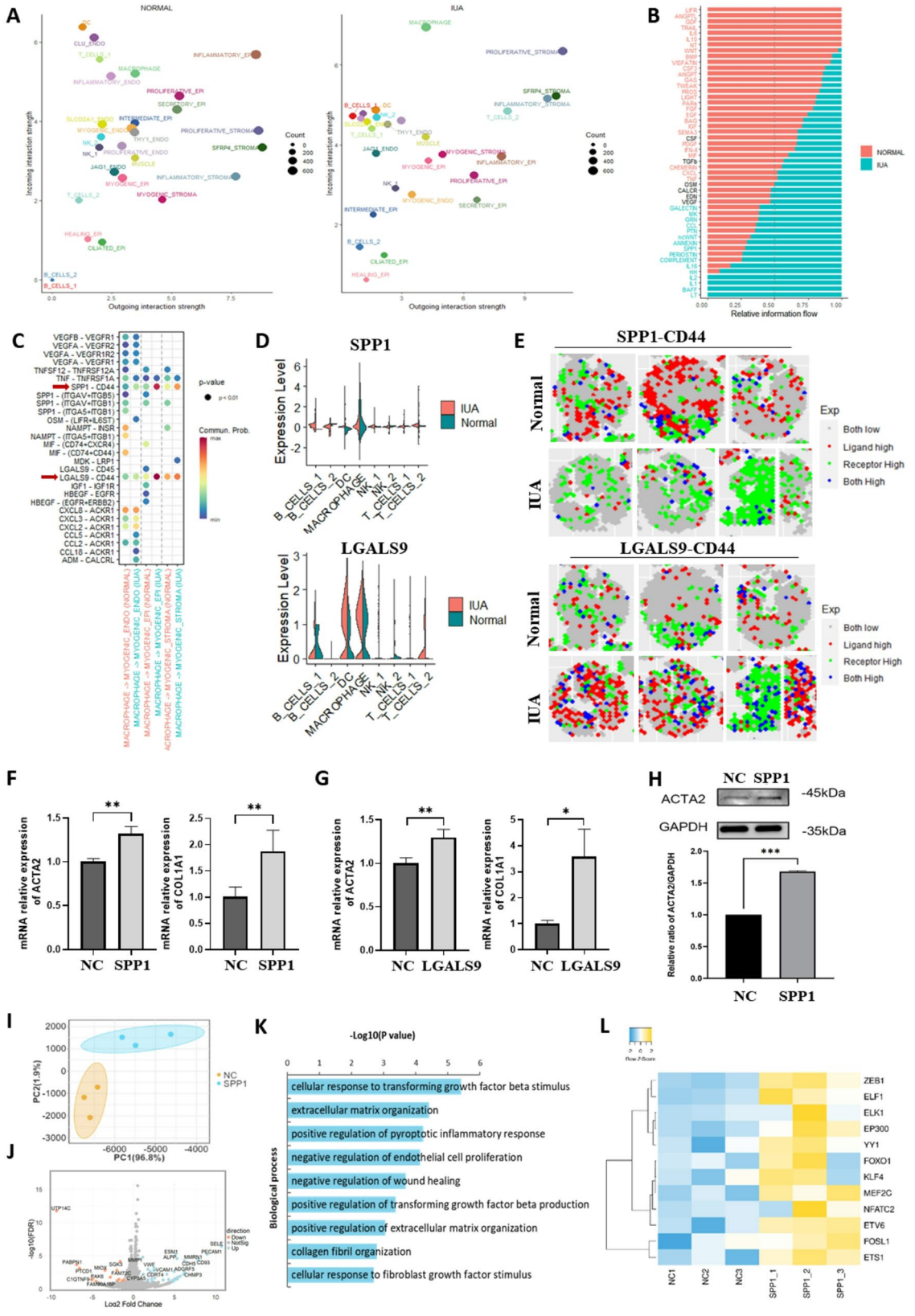


**Fig. 5** (See legend on next page.)

(See figure on previous page.)

**Fig. 5** The multi-lineage interactome in the fibrotic niche of human IUA. **A** Scatter plots showing outgoing and incoming interaction strength of different cell types in IUA and normal endometrium by scRNA-seq. **B** Comparison of the relative information flow of each signaling pathway between IUA and normal endometrium. **C** The interactions of ligand-receptor pairs from macrophages to receptors from three myogenic subsets, including Myogenic_stroma, Myogenic_epithelia and Myogenic_endothelia in normal and IUA endometrium. Red arrows highlight the ligand-receptor pairs upregulated in the IUA group. **D** Wrap plot showing comparative expression level of secretory ligands (SPP1 and LGALS9) in immune cell subsets from normal and IUA endometrium. **E** Visium heatmaps showing spatial transcriptomic co-localization of SPP1 and LGALS9 and their cognate receptor CD44 in normal and IUA endometrium. **F** The pro-fibrotic effect of human recombinant SPP1 on endometrial stromal cells verified by qPCR analysis, n = 4 biological replicates, ** P value<0.01. **G** The pro-fibrotic effect of human recombinant LGALS9/Galectin9 on endometrial stromal cells verified by qPCR analysis, n = 4 biological replicates, * P value<0.05, ** P value<0.01. **H** The pro-fibrotic effect of human recombinant SPP1 on ACTA2 expression of endometrial stromal cells verified by Western Blot analysis, n = 3 biological replicates, *** P value<0.001. **I** PCA plot of endometrial stromal cells colored by groups with and without SPP1 treatment by bulk RNA-seq, n = 3 biological replicates in each group. **J** Volcano plot of differentially expressed genes (DEGs) (log2(FC) >1, FDR < 0.05) between groups with and without SPP1 treatment. Blue color indicates upregulated genes, and yellow color indicates downregulated genes. **K** Gene ontology (GO) categories of up-regulated DEGs in group with SPP1 treatment by bulk RNA-seq. **L** Heatmap of upregulated transcription factors (TFs) in endometrial stromal cells with SPP1 treatment by bulk RNA-seq

stroma and myogenic epithelia in the three fibrotic cell lineages play major roles in promoting fibrosis in the pathogenesis of IUA. We also verified the pro-fibrotic immune microenvironment of IUA with a pro-fibrotic macrophage population highly correlated with IUA disease features. Macrophages can promote fibrotic gene expression in endometrial cells through SPP1 and LGALS9.

Fibrosis occurs due to the excessive deposition of extracellular matrix components by fibroblasts, which are considered the only fibrotic cells in the fibrosis process of IUA [25, 40]. In addition to the existing fibroblasts present in the endometrium, epithelial-to-mesenchymal transition (EMT) is considered an important source of fibroblasts. And EMT was proved to be a key mechanism for the progression of IUA [36, 37, 41]. Our study identified a myogenic epithelial subpopulation and demonstrated that the expression of epithelial characteristic markers decreased and that of stromal cell characteristic markers increased in this subpopulation, exhibiting typical EMT characteristics. In addition, the proportion of this subpopulation increased in the endometrium of the IUA group. Thus, our study further demonstrated that EMT may exacerbate the disease progression of IUA.

A recent study also compared single-cell expression profiles from a human endometrium atlas between control and IUA patients. However, they profiled the cellular and molecular abnormalities present during the secretory phase of IUA patients, with particular attention to the window of implantation (WOI). They also observed the presence of an epithelial cell population called "epithelial-PDGFRA", which expressed a mixed combination of epithelial and stromal markers [42]. Similarly, a KRT5−/KRT17 + epithelial cells were identified in pulmonary fibrosis as retaining canonical epithelial lineage-defining genes (*EPCAM*, *NKX2-1*, and *cytokeratins*) while co-expressing a subset of "typical" mesenchymal genes, including *COL1A1*, *FN1*, and *CDH2* (*N-cadherin*). This distinct epithelial population also expressed multiple fibrotic ECM components [43]. In our study, in addition to myofibroblasts, we identified highly enriched myogenic epithelial cells in the IUA endometrium. This myogenic cell population maintained both the molecular characteristics of the epithelium themselves and the molecular characteristics of myogenic lineages. This myogenic cell populations could express a large number of fibrosis-related TFs and ECM-related components, indicating their ECM-producing fibrotic phenotype and direct involvement in endometrial fibrosis. Thus besides the fibroblast lineage, we revealed another fibrotic cell populations of epithelial lineages in human and rat IUA, which shed light on the multiple origins and contributions of the two fibrotic cell populations in the pathogenesis of IUA.

In the pathological microenvironment, we revealed a dramatic increase in pro-fibrotic macrophages in the IUA endometrium. Macrophages play key roles in the initiation and resolution of fibrosis [10, 44]. Recent studies on the single-cell atlas of IUA pathogenesis also proved the increased number of macrophage populations in the late proliferative [45] phase and secretory phase [42] of IUA. More importantly, our study confirmed a highly positive correlation between macrophage enrichment and clinical disease phenotype of IUA. Several lines of evidence suggest that macrophages can be a source of ligands that promote a fibrotic activation program in fibroblasts through the fibroblast-macrophage interactions [46]. For example, macrophages have been proven to be a major source of TGF-β in muscle and pulmonary fibrosis [47, 48]. TGFβ can induce the expression of various fibrotic factors via SMAD1 and SMAD3 activation downstream [49]. Although TGFβ was not included in the top list of differentially expressed signals in our study, the myogenic cell subpopulations of the three lineages indeed exhibited higher levels of fibrosis-related genes expression and chromosomal accessibility at the *SMAD1* and *SMAD3* gene site. We identified and validated novel pro-fibrotic ligands secreted by macrophages (SPP1 and LGALS9) that interact most significantly with three myogenic cell subpopulations in IUA endometrium. The previous studies proved that SPP1 [50] and LGALS9 [51] can indeed activate SMAD3 signaling.

SPP1 is a consistent biomarker of idiopathic pulmonary fibrosis (IPF) [52]. SPP1 has also been implicated in renal, cardiac, liver and bone marrow fibrosis [53–56]. SPP1 deletion ameliorates dermal fibrosis and lung fibrosis [57, 58], suggesting that SPP1 may have a general role in promoting fibrosis. LGALS9/Galectin9 is a member of the soluble galectin family that shares an affinity for β-galactoside-containing saccharides [59]. LGALS9/Galectin9 has been reported to be prominently expressed in the fibrotic liver [60]. LGALS9/Galectin9 has been highlighted as a mediator of lung fibrosis, and its mechanism of action involves TGFβ signaling [61]. However, no research has proven the role of SPP1 and LGALS9/Galectin9 in endometrial fibrosis. Our study innovatively demonstrated the role of SPP1 and LGALS9/Galectin9 in promoting endometrial fibrosis in IUA, providing new molecular targets for the endometrial fibrosis disease.

Together, our study highlights the multiple myogenic cell lineages contributing to endometrial fibrosis and reveals the fibrotic niche of human IUA at the single-cell level. All cellular and molecular pathological changes showed high consistency in both human and rat IUA endometrium, which provided theoretical guidance for the development of therapeutic targets for IUA.

## Conclusions

In this study, we reconstructed a single-cell multi-omics atlas of human IUA and investigated the diversity of fibrotic cell lineages and pro-fibrotic immune microenvironments in human and rat IUA. We generated a multi-lineage interactome in the fibrotic niche of IUA, in which SPP1 and LGALS9 secreted by macrophages promoted the fibrotic changes in endometrial cells. Our study resolved the conserved multiple fibrotic cell lineages and their pathogenic microenvironments in IUA, and provided therapeutic targets for developing effective strategies for IUA treatment.

### Abbreviations

| | |
|---|---|
| AFS | American Fertility Society |
| AS | Asherman's syndrome |
| cDNA | Complementary deoxyribonucleic acid |
| DC | Dendritic cell |
| DMEM | Dulbecco's Modified Eagle Medium |
| ECM | Extracellular matrix |
| EMT | Epithelial-mesenchymal transition |
| FBS | Fetal bovine serum |
| GO | Gene ontology |
| GSA | Genome Sequence Archive |
| HBSS | Hank's Balanced Salt Solution |
| IF | Immunofluorescence |
| IPF | Idiopathic pulmonary fibrosis |
| IUA | Intrauterine adhesion |
| PC | Principal component |
| PVDF | Polyvinylidene fluoride membrane |
| RT | Reverse transcription |
| scRNA | Seq-single cell RNA sequencing |
| snATAC | Seq-single nucleus transposase-accessible chromatin sequencing |
| SPF | Specific pathogen-free |
| TSS | Transcription start site |
| TF | Transcription factor |
| UMAP | Uniform manifold approximation and projection |
| WOI | Window of implantation |

## Supplementary Information

The online version contains supplementary material available at https://doi.org/10.1186/s13073-026-01641-x.

Supplementary Material 1. Additional file 1: Table S1-S3. Table S1: Clinical samples from different Datasets for single cell analysis; Table S2: cell numbers of each samples before and after QC in scRNA-seq analysis; Table S3: Clinical samples collected for histological analysis

Supplementary Material 2. Additional file 2: Table S4, Gene ontology (GO) terms of marker genes of the myogenic sub-clusters

Supplementary Material 3. Additional file 3: Fig S1-S6. Supplementary figures

### Acknowledgements

This work was supported by the National Natural Science Foundation of China (82371636, 82171616, 82201783), the Zhejiang Provincial Natural Science Foundation of China (LZ22H040001, LBD23H040001, LR24H040001) and the Science and Technology Program of Jinhua Science and Technology Bureau (Grant No. 2021-3-001, 2024-3-123).

### Authors' contributions

Yu Li: experiment validation, data interpretation, manuscript writing; Wei Wu: tissue collection and immunofluorescence staining, manuscript writing; Houyi Lv: Cell culture and in-vitro experiments; Xilin Shen & Yiyuan Qu: data analysis; Libing Shi, Wanwan Xu, Shunxian Ji, Yingying Hu, Xiao Chen, Xiaofeng Zhao: acquisition of sample, sample processing; Junwen Zhang, Ying Gu, Zhuomin Wang, Chengcheng Zhu: animal experiments; Zafar: manuscript preparation; Songying Zhang, Jian Xu: conception and design; Bingbing Wu: conception and design, data analysis and interpretation, manuscript writing; All authors read and approved the final manuscript.

### Funding

This work was supported by the National Natural Science Foundation of China (82371636, 82171616, 82201783), the Zhejiang Provincial Natural Science Foundation of China (LZ22H040001, LBD23H040001, LR24H040001) and the Science and Technology Program of Jinhua Science and Technology Bureau (Grant No. 2021-3-001, 2024-3-123).

### Data availability

The raw data of each single cell generated in this study were deposited in the public database of the Genome Sequence Archive (GSA) [62] under accession numbers [HRA000928] [63] https://ngdc.cncb.ac.cn/gsa-human/submit/hra/subHRA001173/detail and HRA001019 [64] in National Genomics Data Center, China National Center for Bioinformation / Beijing Institute of Genomics, Chinese Academy of Sciences. We integrated the single data generated in this study with scRNA-seq data from six normal human endometrial samples collected from two published datasets, including the ArrayExpress datasets under accession number E-MTAB-10287 and NCBI's Gene Expression Omnibus datasets with series accession code GSE111976. The sample information for the three datasets (our study, E-MTAB-10287 and GSE111976) is shown in Table S1 (Additional file 1). All the code used in this study is publicly available at GitHub (https://github.com/ShenXilin/scIUA) [65].

## Declarations

### Ethics approval and consent to participate

Approvals for utilizing the patient samples were obtained from Ethics Committee of the Fourth Affiliated Hospital, School of Medicine, Zhejiang University (Approval Number: K2021042). Informed consents were obtained from all participants. Approvals for the use of the fixing samples in paraffin wax were obtained from the Ethics Committee of the Fourth Affiliated

Hospital, School of Medicine, Zhejiang University (Approval Number: K2021113). The research conformed to the principles of the Helsinki Declaration. All animal experiments were approved by the Ethics Committee of Zhejiang University (approval no. ZJU20230011).

**Consent for publication**
Not applicable.

**Competing interests**
The authors declare no competing interests.

**Author details**
[1]Department of Obstetrics and Gynecology, Center for Reproductive Medicine, the Fourth Affiliated Hospital of School of Medicine, and International School of Medicine, International Institutes of Medicine, Zhejiang University, N1 Shangcheng Road, Yiwu 322000, China
[2]Dr. Li Dak Sum & Yip Yio Chin Center for Stem Cell and Regeneration Medicine, Zhejiang University, Hangzhou, Zhejiang, China
[3]Assisted Reproduction Unit, Department of Obstetrics and Gynecology, Sir Run Run Shaw Hospital, Key Laboratory of Reproductive Dysfunction Management of Zhejiang Province, Zhejiang University School of Medicine, Hangzhou, China
[4]Women's Hospital, Zhejiang University School of Medicine, Hangzhou, Zhejiang, China

Received: 18 November 2024 / Accepted: 28 March 2026
Published online: 07 April 2026

**References**

1. Hooker AB, Lemmers M, Thurkow AL, Heymans MW, Opmeer BC, Brolmann HA, Mol BW, Huirne JA. Systematic review and meta-analysis of intrauterine adhesions after miscarriage: prevalence, risk factors and long-term reproductive outcome. Hum Reprod Update. 2014;20:262–78.
2. Schenker JG, Margalioth EJ. Intrauterine adhesions: an updated appraisal. Fertil Steril. 1982;37:593–610.
3. Nybo Andersen AM, Wohlfahrt J, Christens P, Olsen J, Melbye M. Maternal age and fetal loss: population based register linkage study. BMJ. 2000;320:1708–12.
4. Quenby S, Gallos ID, Dhillon-Smith RK, Podesek M, Stephenson MD, Fisher J, Brosens JJ, Brewin J, Ramhorst R, Lucas ES, et al. Miscarriage matters: the epidemiological, physical, psychological, and economic costs of early pregnancy loss. Lancet. 2021;397:1658–67.
5. Yu D, Wong YM, Cheong Y, Xia E, Li TC. Asherman syndrome–one century later. Fertil Steril. 2008;89:759–79.
6. Xin L, Lin X, Pan Y, Zheng X, Shi L, Zhang Y, Ma L, Gao C, Zhang S. A collagen scaffold loaded with human umbilical cord-derived mesenchymal stem cells facilitates endometrial regeneration and restores fertility. Acta Biomater. 2019;92:160–71.
7. Lv H, Wu B, Song J, Wu W, Cai W, Xu J. Hydrogel, a novel therapeutic and delivery strategy, in the treatment of intrauterine adhesions. J Mater Chem B. 2021;9:6536–52.
8. Gao M, Yu Z, Yao D, Qian Y, Wang Q, Jia R. Mesenchymal stem cells therapy: A promising method for the treatment of uterine scars and premature ovarian failure. Tissue Cell. 2022;74:101676.
9. Abudukeyoumu A, Li MQ, Xie F. Transforming growth factor-beta1 in intrauterine adhesion. Am J Reprod Immunol. 2020;84:e13262.
10. Henderson NC, Rieder F, Wynn TA. Fibrosis: from mechanisms to medicines. Nature. 2020;587:555–66.
11. Kuppe C, Ibrahim MM, Kranz J, Zhang X, Ziegler S, Perales-Paton J, Jansen J, Reimer KC, Smith JR, Dobie R, et al. Decoding myofibroblast origins in human kidney fibrosis. Nature. 2021;589:281–6.
12. Krenkel O, Hundertmark J, Ritz TP, Weiskirchen R, Tacke F. Single Cell RNA Sequencing Identifies Subsets of Hepatic Stellate Cells and Myofibroblasts in Liver Fibrosis. Cells. 2019;8:503.
13. Driskell RR, Lichtenberger BM, Hoste E, Kretzschmar K, Simons BD, Charalambous M, Ferron SR, Herault Y, Pavlovic G, Ferguson-Smith AC, Watt FM. Distinct fibroblast lineages determine dermal architecture in skin development and repair. Nature. 2013;504:277–81.
14. GK YL. featureCounts: an efficient general purpose program for assigning sequence reads to genomic features. Bioinf (Oxford England). 2014;30:923–30.
15. Satija R, Farrell JA, Gennert D, Schier AF, Regev A. Spatial reconstruction of single-cell gene expression data. Nat Biotechnol. 2015;33:495–U206.
16. Zhou Y, Zhou B, Pache L, Chang M, Khodabakhshi AH, Tanaseichuk O, Benner C, Chanda SK. Metascape provides a biologist-oriented resource for the analysis of systems-level datasets. Nat Commun. 2019;10:1523.
17. Street K, Risso D, Fletcher RB, Das D, Ngai J, Yosef N, Purdom E, Dudoit S. Slingshot: cell lineage and pseudotime inference for single-cell transcriptomics. BMC Genomics. 2018;19:477.
18. Ramilowski JA, Goldberg T, Harshbarger J, Kloppmann E, Lizio M, Satagopam VP, Itoh M, Kawaji H, Carninci P, Rost B, Forrest ARR. A draft network of ligand-receptor-mediated multicellular signalling in human. Nature Communications. 2015;6:7866.
19. Jin S, Guerrero-Juarez CF, Zhang L, Chang I, Ramos R, Kuan CH, Myung P, Plikus MV, Nie Q. Inference and analysis of cell-cell communication using CellChat. Nat Commun. 2021;12:1088.
20. Granja JM, Corces MR, Pierce SE, Bagdatli ST, Choudhry H, Chang HY, Greenleaf WJ. ArchR is a scalable software package for integrative single-cell chromatin accessibility analysis. Nat Genet. 2021;53:403–11.
21. Liu Q, Hsu CY, Shyr Y. Scalable and model-free detection of spatial patterns and colocalization. Genome Res. 2022;32:1736–45.
22. Wang J, Li D, Pan Y, Li J, Jiang Q, Liu D, Hou Y. Interleukin-34 accelerates intrauterine adhesions progress related to CX3CR1(+) monocytes/macrophages. Eur J Immunol. 2021;51:2501–12.
23. Wang W, Vilella F, Alama P, Moreno I, Mignardi M, Isakova A, Pan W, Simon C, Quake SR. Single-cell transcriptomic atlas of the human endometrium during the menstrual cycle. Nat Med. 2020;26:1644–53.
24. Garcia-Alonso L, Handfield LF, Roberts K, Nikolakopoulou K, Fernando RC, Gardner L, Woodhams B, Arutyunyan A, Polanski K, Hoo R, et al. Mapping the temporal and spatial dynamics of the human endometrium in vivo and in vitro. Nat Genet. 2021;53:1698–711.
25. Xu C, Bao M, Fan X, Huang J, Zhu C, Xia W. EndMT: New findings on the origin of myofibroblasts in endometrial fibrosis of intrauterine adhesions. Reprod Biol Endocrinol. 2022;20:9.
26. Wu B, Li Y, Nie N, Shen X, Jiang W, Liu Y, Gong L, An C, Zhao K, Yao X, et al. SFRP4(+) stromal cell subpopulation with IGF1 signaling in human endometrial regeneration. Cell Discov. 2022;8:95.
27. Trapnell C, Cacchiarelli D, Grimsby J, Pokharel P, Li SQ, Morse M, Lennon NJ, Livak KJ, Mikkelsen TS, Rinn JL. The dynamics and regulators of cell fate decisions are revealed by pseudotemporal ordering of single cells. Nat Biotechnol. 2014;32:381–U251.
28. Bai YM, Yang F, Luo P, Xie LL, Chen JH, Guan YD, Zhou HC, Xu TF, Hao HW, Chen B, et al. Single-cell transcriptomic dissection of the cellular and molecular events underlying the triclosan-induced liver fibrosis in mice. Mil Med Res. 2023;10:7.
29. Zhang LY, Tan Y, Luo XJ, Wu JF, Ni YR. The roles of ETS transcription factors in liver fibrosis. Hum Cell. 2023;36:528–39.
30. Li J, Yang Y, Li Q, Wei S, Zhou Y, Yu W, Xue L, Zhou L, Shen L, Lu G, et al. STAT6 contributes to renal fibrosis by modulating PPARα-mediated tubular fatty acid oxidation. Cell Death Dis. 2022;13:66.
31. Tabib T, Huang M, Morse N, Papazoglou A, Behera R, Jia M, Bulik M, Monier DE, Benos PV, Chen W, et al. Myofibroblast transcriptome indicates SFRP2(hi) fibroblast progenitors in systemic sclerosis skin. Nat Commun. 2021;12:4384.
32. Muñoz-Félix JM, González-Núñez M, López-Novoa JM. ALK1-Smad1/5 signaling pathway in fibrosis development: friend or foe? Cytokine Growth Factor Rev. 2013;24:523–37.
33. Chan SC, Zhang Y, Shao A, Avdulov S, Herrera J, Aboudehen K, Pontoglio M, Igarashi P. Mechanism of Fibrosis in HNF1B-Related Autosomal Dominant Tubulointerstitial Kidney Disease. J Am Soc Nephrol. 2018;29:2493–509.
34. Rockey DC, Bell PD, Hill JA. Fibrosis–a common pathway to organ injury and failure. N Engl J Med. 2015;372:1138–49.
35. Salma U, Xue M, Ali Sheikh MS, Guan X, Xu B, Zhang A, Huang L, Xu D. Role of Transforming Growth Factor-β1 and Smads Signaling Pathway in Intrauterine Adhesion. Mediators Inflamm. 2016;2016:4158287.
36. Yao Y, Chen R, Wang G, Zhang Y, Liu F. Exosomes derived from mesenchymal stem cells reverse EMT via TGF-beta1/Smad pathway and promote repair of damaged endometrium. Stem Cell Res Ther. 2019;10:225.
37. Chen Y, Sun D, Shang D, Jiang Z, Miao P, Gao J. miR-223-3p alleviates TGF-beta-induced epithelial-mesenchymal transition and extracellular matrix

deposition by targeting SP3 in endometrial epithelial cells. Open Med (Wars). 2022;17:518–26.
38. Qian W, Cai X, Qian Q, Peng W, Yu J, Zhang X, Tian L, Wang C. lncRNA ZEB1-AS1 promotes pulmonary fibrosis through ZEB1-mediated epithelial-mesenchymal transition by competitively binding miR-141-3p. Cell Death Dis. 2019;10:129.
39. Moreno I, Capalbo A, Mas A, Garrido-Gomez T, Roson B, Poli M, Dimitriadis E, Santamaria X, Vilella F, Simon C. The human periconceptional maternal-embryonic space in health and disease. Physiol Rev. 2023;103:1965–2038.
40. Rosenbloom J, Castro SV, Jimenez SA. Narrative review: fibrotic diseases: cellular and molecular mechanisms and novel therapies. Ann Intern Med. 2010;152:159–66.
41. Zhao G, Li R, Cao Y, Song M, Jiang P, Wu Q, Zhou Z, Zhu H, Wang H, Dai C, et al. ΔNp63α-induced DUSP4/GSK3β/SNAI1 pathway in epithelial cells drives endometrial fibrosis. Cell Death Dis. 2020;11:449.
42. Santamaria X, Roson B, Perez-Moraga R, Venkatesan N, Pardo-Figuerez M, Gonzalez-Fernandez J, Llera-Oyola J, Fernández E, Moreno I, Salumets A, et al. Decoding the endometrial niche of Asherman's Syndrome at single-cell resolution. Nat Commun. 2023;14:5890.
43. Habermann AC, Gutierrez AJ, Bui LT, Yahn SL, Winters NI, Calvi CL, Peter L, Chung MI, Taylor CJ, Jetter C, et al. Single-cell RNA sequencing reveals pro-fibrotic roles of distinct epithelial and mesenchymal lineages in pulmonary fibrosis. Sci Adv. 2020;6:eaba1972.
44. Wynn TA, Barron L. Macrophages: master regulators of inflammation and fibrosis. Semin Liver Dis. 2010;30:245–57.
45. Lv H, Sun H, Wang L, Yao S, Liu D, Zhang X, Pei Z, Zhou J, Wang H, Dai J, et al. Targeting CD301(+) macrophages inhibits endometrial fibrosis and improves pregnancy outcome. EMBO Mol Med. 2023;15:e17601.
46. Buechler MB, Fu W, Turley SJ. Fibroblast-macrophage reciprocal interactions in health, fibrosis, and cancer. Immunity. 2021;54:903–15.
47. Juban G, Saclier M, Yacoub-Youssef H, Kernou A, Arnold L, Boisson C, Ben Larbi S, Magnan M, Cuvellier S, Théret M, et al. AMPK Activation Regulates LTBP4-Dependent TGF-β1 Secretion by Pro-inflammatory Macrophages and Controls Fibrosis in Duchenne Muscular Dystrophy. Cell Rep. 2018;25:2163–e21762166.
48. Young LR, Gulleman PM, Short CW, Tanjore H, Sherrill T, Qi A, McBride AP, Zaynagetdinov R, Benjamin JT, Lawson WE, et al. Epithelial-macrophage interactions determine pulmonary fibrosis susceptibility in Hermansky-Pudlak syndrome. JCI Insight. 2016;1:e88947.
49. Frangogiannis N. Transforming growth factor-β in tissue fibrosis. J Exp Med. 2020;217:e20190103.
50. Faqeer A, Wang M, Alam G, Padhiar AA, Zheng D, Luo Z, Zhao IS, Zhou G, van den Beucken J, Wang H, Zhang Y. Cleaved SPP1-rich extracellular vesicles from osteoclasts promote bone regeneration via TGFβ1/SMAD3 signaling. Biomaterials. 2023;303:122367.
51. Wu C, Thalhamer T, Franca RF, Xiao S, Wang C, Hotta C, Zhu C, Hirashima M, Anderson AC, Kuchroo VK. Galectin-9-CD44 interaction enhances stability and function of adaptive regulatory T cells. Immunity. 2014;41:270–82.
52. Morse C, Tabib T, Sembrat J, Buschur KL, Bittar HT, Valenzi E, Jiang Y, Kass DJ, Gibson K, Chen W et al. Proliferating SPP1/MERTK-expressing macrophages in idiopathic pulmonary fibrosis. Eur Respir J. 2019;54:1802441.
53. Collins AR, Schnee J, Wang W, Kim S, Fishbein MC, Bruemmer D, Law RE, Nicholas S, Ross RS, Hsueh WA. Osteopontin modulates angiotensin II-induced fibrosis in the intact murine heart. J Am Coll Cardiol. 2004;43:1698–705.
54. Merszei J, Wu J, Torres L, Hicks JM, Bartkowiak T, Tan F, Lou YH. Osteopontin overproduction is associated with progression of glomerular fibrosis in a rat model of anti-glomerular basement membrane glomerulonephritis. Am J Nephrol. 2010;32:262–71.
55. Ruberti S, Bianchi E, Guglielmelli P, Rontauroli S, Barbieri G, Tavernari L, Fanelli T, Norfo R, Pennucci V, Fattori GC, et al. Involvement of MAF/SPP1 axis in the development of bone marrow fibrosis in PMF patients. Leukemia. 2018;32:438–49.
56. Ouyang JF, Mishra K, Xie Y, Park H, Huang KY, Petretto E, Behmoaras J. Systems level identification of a matrisome-associated macrophage polarisation state in multi-organ fibrosis. Elife. 2023;12:e85530.
57. Dong J, Ma Q. Osteopontin enhances multi-walled carbon nanotube-triggered lung fibrosis by promoting TGF-β1 activation and myofibroblast differentiation. Part Fibre Toxicol. 2017;14:18.
58. Wu M, Schneider DJ, Mayes MD, Assassi S, Arnett FC, Tan FK, Blackburn MR, Agarwal SK. Osteopontin in systemic sclerosis and its role in dermal fibrosis. J Invest Dermatol. 2012;132:1605–14.
59. Mariño KV, Cagnoni AJ, Croci DO, Rabinovich GA. Targeting galectin-driven regulatory circuits in cancer and fibrosis. Nat Rev Drug Discov. 2023;22:295–316.
60. Fujita K, Niki T, Nomura T, Oura K, Tadokoro T, Sakamoto T, Tani J, Yoneyama H, Morishita A, Kuroda N, et al. Correlation between serum galectin-9 levels and liver fibrosis. J Gastroenterol Hepatol. 2018;33:492–9.
61. Hsu YA, Chang CY, Lan JL, Li JP, Lin HJ, Chen CS, Wan L, Liu FT. Amelioration of bleomycin-induced pulmonary fibrosis via TGF-β-induced Smad and non-Smad signaling pathways in galectin-9-deficient mice and fibroblast cells. J Biomed Sci. 2020;27:24.
62. Zhang S, Chen X, Jin E, Wang A, Chen T, Zhang X, Zhu J, Dong L, Sun Y, Yu C et al. The GSA Family in 2025: A Broadened Sharing Platform for Multi-omics and Multimodal Data. Genomics Proteom Bioinf. 2025;23:qzaf072.
63. Wu BB, Li Y, Wu W, Lv HY, Shi LB, Wang ZM, Zhu CC, Zhang JW, Shen XL, Qu YY, Xu WW, Ji SX, Gu Y, Zafar MI, Hu YY, Chen X, Zhao XF, Zhao SY, Xu J. Single cell multiomics revealed fibrotic trajectories of endometrial cells and interaction with the pro-fibrotic macrophages in intrauterine adhesion. HRA000928. Genome Sequence Archive. 2026. https://ngdc.cncb.ac.cn/gsa-human/browse/HRA000928
64. Wu BB, Li Y, Wu W, Lv HY, Shi LB, Wang ZM, Zhu CC, Zhang JW, Shen XL, Qu YY, Xu WW, Ji SX, Gu Y, Zafar MI, Hu YY, Chen X, Zhao XF, Zhao SY, Xu J. Single cell multiomics revealed fibrotic trajectories of endometrial cells and interaction with the pro-fibrotic macrophages in intrauterine adhesion. HRA001019. Genome Sequence Archive. 2026. https://ngdc.cncb.ac.cn/gsa-human/browse/HRA001019
65. Wu BB, Li Y, Wu W, Lv HY, Shi LB, Wang ZM, Zhu CC, Zhang JW, Shen XL, Qu YY, Xu WW, Ji SX, Gu Y, Zafar MI, Hu YY, Chen X, Zhao XF, Zhao SY, Xu J. Single cell multiomics revealed fibrotic trajectories of endometrial cells and interaction with the pro-fibrotic macrophages in intrauterine adhesion. GitHub. 2026. https://github.com/ShenXilin/scIUA

## Publisher's note